

RiskMap: A Unified Driving Context Representation for Autonomous Motion Planning in Urban Driving Environment

Ren Xin¹, Sheng Wang¹, Yingbing Chen¹, Jie Cheng² and Ming Liu^{1,2}

Abstract—Planning is complicated by the combination of perception and map information, particularly when driving in heavy traffic. Developing an extendable and efficient representation that visualizes sensor noise and provides constraints to real-time planning tasks is desirable.

We aim to develop an extendable map representation offering prior to cost in planning tasks to simplify the planning process of dealing with complex driving scenarios and visualize sensor noise. In this paper, we illustrate a unified context representation empowered by a modern deep learning motion prediction model, representing statistical cognition of motion prediction for human beings. A sampling-based planner is adopted to train and compare the difference in risk map generation methods. The training tools and model structures are investigated illustrating their efficiency in this task.

I. INTRODUCTION

Deep Neural Network(DNN) is widely used to approximate high-dimensional feature functions that are hard to mathematically describe. It is proven to be able to approximate any Lebesgue Integrable function with sufficient parameters and proper structure [1].

However, millions of parameters make deep neural networks difficult to analyze and interpret. At the same time, traditional analytical planning methods, including optimization and sampling, are only reliable in limited scenarios. This paper presents an effective and interpretable method for combining the advantage of traditional and deep learning-based approaches.

A. Motivation

Planning under constraints of traffic environment and predicted motions of other vehicles is a typical strategy for autonomous vehicles(AV). For prediction, a network-based probabilistic model seems more competent as the maneuver of the agent in traffic is full of uncertainties. It's possible that at some point other traffic participants will do something outside the rules. However, the planning module, as an actor, should not make maneuvers beyond the rules. But an end-to-end neural network planner is hard to treat curb or traffic rules as hard constrain. It is commonly observed to lead to curb-violated results. Thus, the planning process may be considered a deterministic decision process regulated by hard constraints, rather than a probabilistic model.

¹Ren Xin, Sheng Wang, Yingbing Chen and Ming Liu are with The Hong Kong University of Science and Technology (Guangzhou), Thrust of Robotics & Autonomous Systems, Guangdong, China. {rxin, swangei, ychengz}@connect.ust.hk.

²Jie Cheng and Ming Liu are with The Hong Kong University of Science and Technology, Department of Electronic and Computer Engineering, Clear Water Bay, Kowloon, Hong Kong SAR, China. {jchengai}@connect.ust.hk, eelium@ust.hk.

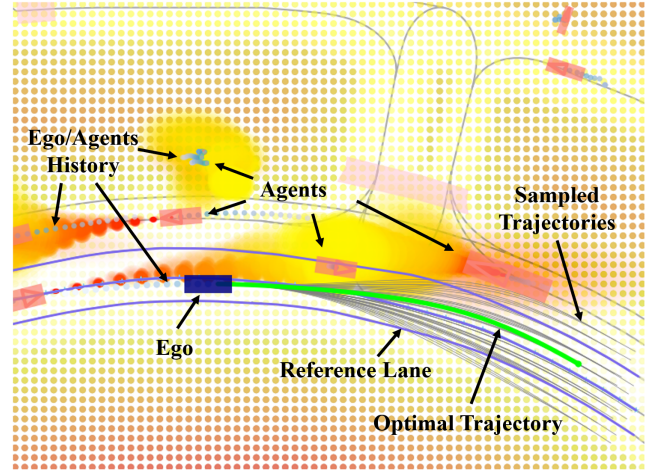


Fig. 1: Planning under urban scenarios is a challenging task because it needs to consider the perception, prediction, and control uncertainties together with complex road environments. Our method reflects all perception information in a risk map, which is a middleware of sensing and planning. The purple rectangle represents the ego vehicle, the red blocks are other agents. The transparency of **orange-yellow** fields represents the occupancy probability of other traffic participants. The **white-yellow-orange** points represent the risk value of sampled positions. Sample points with higher risk values are redder.

In a prediction-planning decoupling framework, ensuring the rich and efficient expression of prediction results [2], [3], as well as sufficient interpretability and flexibility of the planning module [2], [4], [5] are important. Therefore, methods of mapping circumstance information to risk space and best-cost trajectory selection mechanisms are explored.

B. Challenges

The Representation and Utilization of Prediction Results. Modern HD map, cognition, and prediction methods offer plentiful driving context information, including reference lanes, traffic lights, occupancy maps, and multi-modal future trajectories with probability. Interactive planning methods with multi-modal prediction are inspected in [6], [7]. Previous works [2], [3] draw on the concept of flow commonly used in motion perception to predict the position of other traffic participants, while no explicit utilization is developed.

Regularization of Cost Function To address the upper problems, the deep learning-based cost function is intro-

duced. However, directly minimizing the cost of expert trajectory will result in letting all the sampled states at a small value rather than just making the trajectory the optimum. So loss terms regularizing the cost value is in need.

C. Contribution

To solve the above issues and increase flexibility and interpretability in planning, we propose the RiskMap framework. To the best knowledge of us, this method is the first to generate interpretable unified driving context representation in risk space by imitation learning. Our contributions are mainly three folds:

(1) We propose a novel generator of differential signed risk field which is an analytical representation of probabilistic prediction distribution for downstream planning tasks.

(2) We propose a real-time planner that generates smooth and human-like trajectories with RiskMap outputs.

(3) We integrate RiskMap and planner together proofing the efficiency of map generating modules and the effectiveness of modeling tools.

II. RELATED WORK

A. Driving Motion Prediction

Traditional rule-based behavior prediction methods generate multiple possible trajectories based on constraints from road maps. Thanks to the great development of deep learning, more recently, many learning-based approaches are proposed [8], [9], they take the rasterized map information and vehicle history trajectory as input and output different hypotheses mean while assigning the possibilities to each of them.

Some other methods [10], [11] choose to encode contextual information by vector format which is more powerful since its more efficient context representing ability. In addition, they use the attention mechanism or graph convolution method to aggregate information and learn the latent interaction model so that the predictor can pay more attention to the information most related.

To generate diverse possible predictions, some generative, probabilistic approaches [12], [13] based on variational autoencoder(VAE) [14] learn to directly output distribution of potential future trajectories instead of focus on the best possible trajectory. This is more friendly to the downstream planning task as it also outputs the variance, which can be used to make more reasonable decisions.

Recently, some works [15] focus on introducing prior domain knowledge to make prediction results more accurate and reasonable. Jie *et al.* [16] emphasizes reference lane in context presentation to enhance the success rate and planning diversity.

B. Representation of Map Information

The map is of vital importance for mobile robots [17]. It is an integration cognition result. The concept of occupancy grid map [18] and configuration space simplified the problem of mobile robots in the past tens of years. The utilization of the signed distance field algorithm in 2D static maps efficiently offers gradient in trajectory optimization tasks.

Rasterize probabilistic occupancy map [19] is adopted to improve target position distribution rationality. HD maps [20] offering a variety of semantic information is essential for modern urban autonomous driving. The occupancy flow is developed for predicting the motion potential in a driving scenario [2], [3] but, to our knowledge, no analytical planning algorithm based on it is demonstrated for now.

The risk map is not a brand-new concept. Risk is defined as the collision probability in the future [21]. Nishimura *et al.* [6] introduced prediction entropy as an optimization item of Model Predictive Control(MPC). Risk combination methods and threshold estimation are discussed in [22], [23]. Huang *et al.* [22] obtain obstacle uncertainty from traditional perception models and discussed combination methods of risk value of obstacles. Pan *et al.* [24] treat agents' future motion of long and short time horizons in two modes to get more safe trajectory.

C. Inverse Optimal Control and Imitation Learning

There are several main branches of Learning from experts, Inverse Optimal Control(IOC), Behavior Clone(BC), and Inverse Reinforcement Learning(IRL). IOC is to construct a cost function under a relatively stable system, while inverse IRL is to recover a cost function based on a deep neural network in relatively complex systems [25]. In 1826 Abel first, mathematically studied the inverse mechanical problems for finding the curve of an unknown path [26]. Discrete-time IOC scheme for trajectory tracking of non-linear systems is developed by [27]. Levine *et al.* [28], [29] represent the reward function as a Gaussian Process(GP) that maps measurements from feature values to rewards, which inspired me to use exponential to uniform measurements.

Both BC and IRL can be categorized as Imitation Learning. Thanks to the development of parallel programming, large-scale neural networks are becoming more and more widely used. BC directly establishes a mapping from inputs to action, while IRL is trying to find a reward function for behavior decisions.

Previous works [2], [30], [31] combine end-to-end learning with a classical sampling-based planner, either by estimating a cost volume or predicting diverse future trajectories of other agents. However, their results are unreproducible due to the use of a private dataset.

III. METHODOLOGY

A. Problem Formulation

This task is to generate a set of future trajectory points of the ego vehicle $\mathbf{P} = [p^1, \dots, p^T]$ in a short time period T subject to history tracking data of other agents h_a and ego vehicle h_e , map information of current time \mathcal{M} include reference lane m_{ref} , traffic light status m_{tl} , and static obstacles m_{ob} . The driving context is denoted as $\mathcal{S} = (h_a, h_e, \mathcal{M})$ and our model is to find a mapping relationship $\mathbf{P} = \mathcal{F}(\mathcal{S})$.

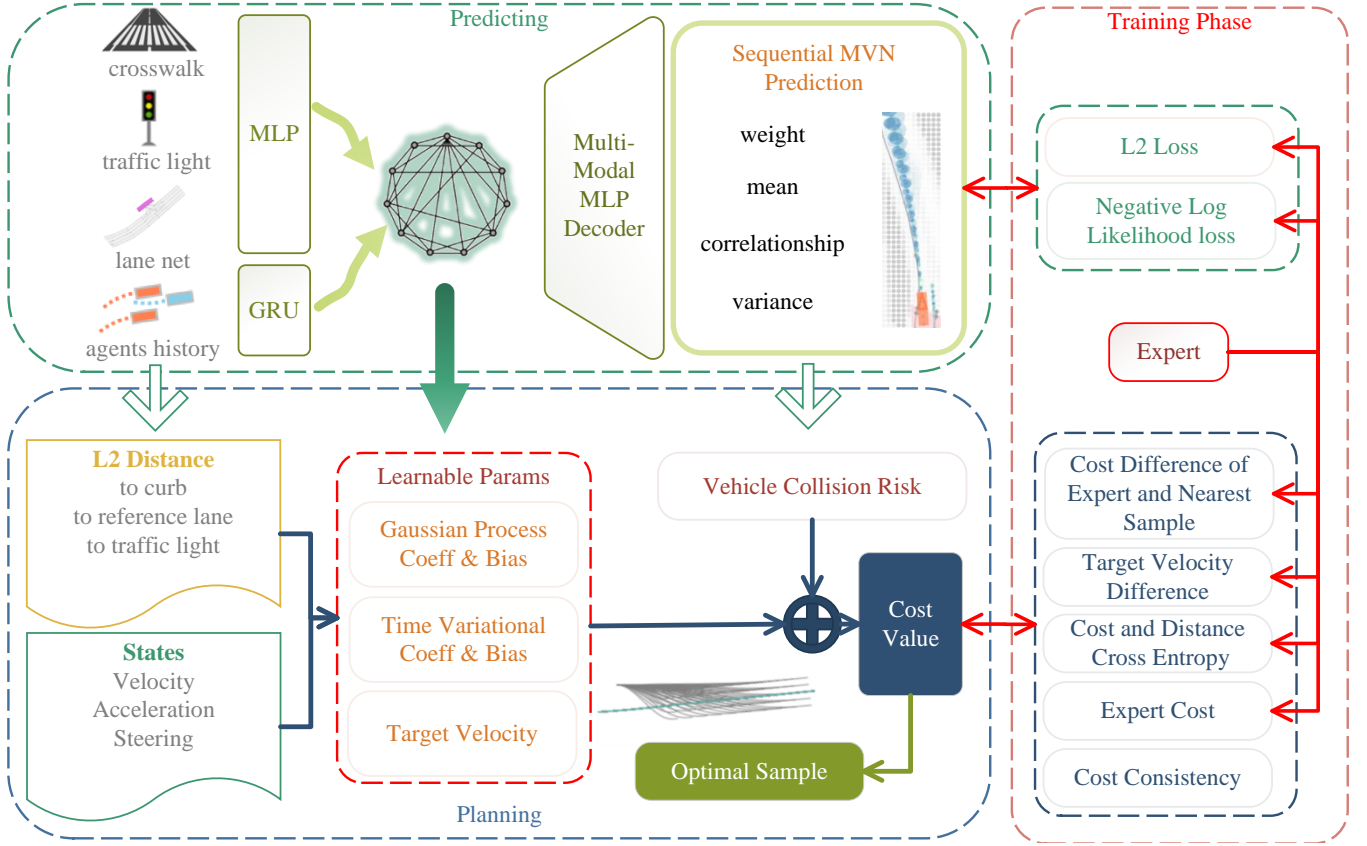


Fig. 2: Illustration of the proposed framework of map generation and planning module with their training process. The framework is roughly divided into two modules: prediction and planning. **Predicting:** Reference lines, map elements, ego & agents motion, and geometry are encoded with MLP/GRU modules. Global attention is used to model the interaction between objects. The multi-modal MLP decoder generates a series of multivariate normal distribution parameters to represent the vehicle future positions. **Planning:** A sampling-based planner is adopted, and all the sampled spatial-temporal points are with distance information to representative represent driving contexts. The global encoded latent variable in the prediction module generates parameters mapping distance to risk value space. Risk values are concatenated with collision risk. The trajectory with the minimum risk is selected as the planning result. **Training:** A two-stage supervised learning process is adopted. The predictor and planner are trained with listed metrics respectively.

B. Driving Context Encoding

Similar to Vectornet [10], a graph neural network is implemented to encode vectorized context information for the prediction module. Both T time step ego-vehicle history $h_e \in \mathbb{R}^{T \times 5}$ and N_a surrounding vehicles $h_a \in \mathbb{R}^{N_a \times T \times 6}$ features are concatenated together and embedded by Gated Recurrent Unit (GRU) to encode the time dimension information. Then the features extracted in 192-dimensional space are processed by a multi-layer perceptron (MLP). Map elements like piecewise lanes and crosswalks poly-line are initially directly encoded by MLP. All the 192-dimensional encoded features are concatenated in the first dimension and aggregated by a global multi-head attention network (GAT) to get the vehicle-to-vehicle and vehicle-to-context relationships.

C. Prediction Results Representation

The presentation method is modeled as Sequential Multi-Variational Normal (SeqMVN) distribution as Fig.3. A tuple

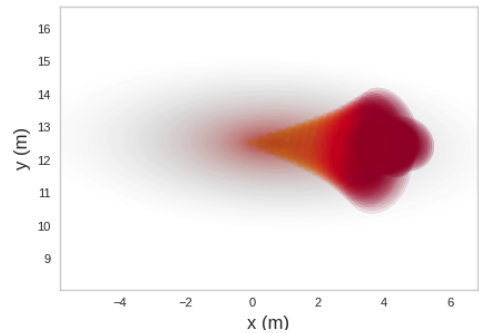


Fig. 3: Demonstration of SeqMVN, deeper color represents later time and the transparency represents the occupancy probability. The image shows that the multi-modality of SeqMVN helps to fit the complex shape of the probabilistic occupancy map. And the Gaussian distribution at different time points in each modal is correlated.

$\mathcal{T}_{mt} = (\mu_x, \mu_y, \sigma_x, \sigma_y, \rho)$ for each trajectory point is generated to present the predicted position center and uncertainty of a vehicle regarding to (1). To ensure the prediction is temporal conditioned on each of their multi-modal results, the overall output is $\mathcal{T} \in \mathbb{R}^{N_a \times N_{modal} \times T \times \dim(\mathcal{P}_{mt})}$ and selection probability $Cl_s \in \mathbb{R}^{N_a \times N_{modal}}$ which can also be considered as weight of Gaussian Mixture Model (GMM) components at a time step for one modal. The likelihood of demo trajectory point \mathcal{T}_{demo}^t is

$$f(\mathcal{T}_{demo}^t) = Cl_s^t \frac{\exp(-\frac{1}{2}(\mathcal{T}_{demo}^t - \boldsymbol{\mu})^T \boldsymbol{\Sigma}^{-1}(\mathcal{T}_{demo}^t - \boldsymbol{\mu}))}{\sqrt{(2\pi)^k |\boldsymbol{\Sigma}|}}, \quad (1)$$

where

$$\boldsymbol{\mu} = \begin{pmatrix} \mu_x \\ \mu_y \end{pmatrix}, \quad \boldsymbol{\Sigma} = \begin{pmatrix} \sigma_x^2 & \rho\sigma_x\sigma_y \\ \rho\sigma_x\sigma_y & \sigma_y^2 \end{pmatrix}, \quad (2)$$

which will avoid the backward tracking problem of different agents [3]. To make sure the distribution is non-degenerate, the output of the MLP-based decoder at σ and ρ position are regularized by exponential and hyperbolic tangent respectively.

Sampling is essential for training the prediction model with uncertainty. Reparameterization is utilized to get the loss for each agent, similar to [8] to cover the gradient fault problem of sampling in backward propagation. Negative Log Likelihood loss (NLL loss) is adopted. The likelihood of ground truth points of an agent is $\mathcal{P}_{mt}^a \in \mathbb{R}^{N_a \times M \times T}$ is calculated by (1). Vanish of each letter represents summation up along that dimension, sum along time horizon is presented as $\mathcal{P}_m^a \in \mathbb{R}^{N_a \times M}$. The optimization target of the prediction stage of each agent is defined as

$$\mathcal{L}_{pre}^a = \sum_{m=1}^M -\log(\mathcal{P}_m^a) - \log(Cl_s^a [\operatorname{argmin}(\|\mathcal{T}_{pre}^a - \mathcal{T}_{demo}^a\|_2)]), \quad (3)$$

where the first item means minimum NLL loss between expert trajectory and predicted trajectory, and the second item means maximizing the probability of selecting the closest prediction modal.

D. Measurement of Driving Context

The boundary of the ego vehicle is presented by a multi-circle model according to their lengths. All the following distances are calculated minus the nearest circle radius. Three Euler distances are measured, the distance to the closest reference lane d_{ref} , the distance to the traffic light d_{tl} , and the distance to static traffic obstacles d_{sdf} . The raw measurements are denoted as $\mathcal{D} = [d_{ref}, d_{sdf}, d_{tl}]$. The elements are mapped to the value space of the signed risk map by

$$\mathcal{R}_{\mathcal{D}} = \beta * \exp(\lambda * \mathcal{D}), \quad (4)$$

where β and λ are generated by an MLP regarding each encoded context feature. The probability of collision with dynamic vehicles of each sample at time step t is

$$\mathcal{R}_{col} = \mathcal{P}_t, \quad (5)$$

The gathered four dim probabilistic feature on each sampled trajectory point $\mathcal{R} = \{\mathcal{R}_{\mathcal{D}}, \mathcal{R}_{col}\}$ is named RiskMap.

E. Design of Cost Function

Weight vectors are generated by MLPs regarding each aggregated context feature. Symbol w_{smooth} represents that preference of driving smoothness $C_{smooth} = (a, s) * w_{smooth}$. Second-order smoothness parameters, including acceleration a and steering s , represent yaw rate differed by ground truth and sampled trajectory. The sampled trajectories are generated by a lattice planner [32], [33]. Difference between expected target velocity \bar{v} and current velocity v $d_v = \bar{v} - v$ is also taken into consideration, where \bar{v} is generated by a swallow decoder. The measurement feature vector is concatenated together. The cost of each trajectory is

$$\mathcal{C}_S = \operatorname{cat}(\mathcal{R}, C_{smooth}, d_v \times w_d), \quad (6)$$

where w_d is a coefficient of velocity difference learned by the model.

F. Loss Definition During Training Process

Excluding minimizing the driving cost, expected velocity \bar{v} is individually regressed by

$$\mathcal{L}_v = \sum_{t=0}^T (\bar{v}^t - v_{\mathcal{T}_{demo}}^t)^2, \quad (7)$$

regulating items that are used to avoid over-fitting is introduced. The selection item calculates Cross Entropy (CE) of cost distribution and distance distribution of sampling trajectory set \mathcal{T}_s by

$$\mathcal{L}_{sel} = CE(\operatorname{Softmin}(\mathcal{C}_{\mathcal{T}_s}), \operatorname{Softmin}(\|\mathcal{S}_s - \mathcal{T}_{demo}\|_2)). \quad (8)$$

Regression item finds the cost difference between selected trajectory and expert trajectory by

$$\mathcal{L}_{l2} = \sum_{t=0}^T \mathcal{C}_{\mathcal{T}_{nearest}}^t - \mathcal{C}_{\mathcal{T}_{demo}}^t. \quad (9)$$

However, all the loss items above will mislead the model to get similar cost values. So a loss item minimizing cost consistency is designed as

$$\mathcal{L}_{con} = \operatorname{Var}(\mathcal{C}_{\mathcal{T}})^{-1}. \quad (10)$$

The overall loss is

$$\mathcal{L} = \mathcal{C}_{\mathcal{T}_{demo}} + \mathcal{L}_{sel} + \mathcal{L}_{l2} + \mathcal{L}_{con} + \mathcal{L}_v. \quad (11)$$

G. Training and Inference Details

A two-stage supervised learning process is conducted. We first train the prediction model from all the vehicles, like the general multi-agent training process. Then the map parameter and cost function training process is conducted by imitating the behavior demo of the ego vehicle. The raw context information is processed the same as in the first stage, and prediction results are inputs of the second stage.

TABLE I: Comparison with Imitation Learning

| Method | ADE (m) | Collision Rate(%) | | | Jerk(m/s ³) |
|-----------------|--------------|-------------------|-------------|-------------|-------------------------|
| | | 1.0s | 2.0s | 3.0s | |
| ChaufferNet | 0.943 | 0.33 | 0.56 | 0.83 | 1.917 |
| ChaufferNet-Vec | 0.475 | 0.31 | 0.49 | 0.71 | 2.679 |
| RiskMap(ours) | 1.084 | 0.00 | 1.31 | 3.17 | 0.2107 |

TABLE II: Ablation Study of Model

| Risk | LN | TV | Samp. Count | ADE (m) | FDE Lat.(m) | FDE Lon.(m) | Jerk (m/s ³) |
|------|----|----|-------------|-------------|-------------|-------------|--------------------------|
| ✓ | | | 400 | 1.16 | 1.48 | 2.01 | 0.2060 |
| | ✓ | ✓ | 400 | 1.99 | 1.63 | 3.78 | 0.2301 |
| ✓ | | ✓ | 100 | 1.17 | 1.85 | 1.84 | 0.2115 |
| ✓ | | ✓ | 400 | 1.08 | 1.88 | 1.57 | 0.2107 |
| ✓ | | ✓ | 900 | 1.07 | 1.90 | 1.53 | 0.2111 |

IV. EXPERIMENT

A. Implementation details

1) *Dataset*: Both the two training stages of our model are conducted on the Lyft Motion Prediction Dataset [34], which contains 134k, 25s time horizon, real-world driving samples, collected on a complex urban route in Palo Alto, California. HD maps and annotations for traffic signals/participants are provided at 10 Hz. A subset of about 3.6M frames is randomly selected for training and tested on a subset of the original validation set which contains 3600 frames.

2) *Training*: We train the prediction model using AdamW [35] optimizer using a batch size of 128 and a learning rate of 1e-4 for 18 epochs on a single RTX 3080 Lap-Top GPU. The planning RiskMap model is trained on 1/10 of the subset for one epoch on the same device. No dataset augmentation is implemented on either of the training stages. We train both the prediction model and RiskMap model to show trajectories for 3 seconds in the future, given the last 1.5 seconds of observation.

3) *Evaluation*: We run our model and other baselines on the logged data and report several common metrics including Average Distance Error(ADE), Final Distance Error(FDE) (Lat. and Lon. are short for lateral and longitudinal offset), Collision Rate, and Jerk(m/s³). The average operation time of generating a planning result is 0.048s(Min. 0.017, Max. 0.111). The operating time meets the real-time requirement.

B. Comparison with Baselines

We compare the planning results against two representative baselines on the Lyft dataset. *ChaufferNet* [36], where

the input is rasterized images and perturbation is used to deal with covariate shift. *ChaufferNet-Vec*, where the rasterized image input is replaced with the recent more advanced vectorized representation [10]. The comparison result are listed in Table I. The baselines are selected to show imitation learning performance. From where we know our method has the lowest Jerk value as it is strictly following dynamic rules and the sampling module offers Jerk optimized trajectories.

C. Ablation Study of Model Components

Table II compares the performance of different module features. **Risk** is our proposed method of mapping Euler distance to risk space by (4). **LN** is to replace the Probabilistic module with a Linear scalar and bias. **TV** is to use temporal parameters on the planning time horizon. No check mark under this item means the model adopts a constant parameter along each time step of sampled trajectories. Different sampling count is tested to verify the extendability of our model. The sampling count only changes the sampling density of a fixed speed and steering range. From rows 1, 2, and 4(our standard model), we can see our proposed method with the same sampling count performs the best on ADE, FDE(Lon.), and Jerk metrics. The time variational mapping params can increase the performance of AED by 7.4%. And the ADE incrementation of the probabilistic model is 84.2% w.r.t Linear model. Rows 3,4,5 shows the performance of the map model will be influenced by downstream planning methods, higher sampling density will achieve better performance without additional training process, but users need to balance the performance and calculation resources.

D. Ablation Study of Loss Items

The results of the Loss items ablation study are listed in Table III. Only one item is removed in each ablation study. The baseline model which adopts all the loss items is listed in row 4 of Table II. Removing *Ind. Vel. Reg.* means the model change the mode of learning target from ground truth to directly learn from sampled costs, as velocity difference is also a cost item. The result shows training loss gets divergent. From the table we find Cross Entropy loss can improve ADE performance by 22.2%, Cost Consistency loss item makes the progress of 14.8%. Cost Regression, in theory, will make the results of the model more robust, but in our small data quantity experiments, we obtain better results than the baseline model of 4.6%. Minimizing Demo cost is an intuitive loss item but it actually draws back the ADE performance of 9.2%. This target may lead to a local minimum of the optimization process of the model.

TABLE III: Ablation Study of Loss Items

| Removed Loss Item | ADE (m) | FDE Lat.(m) | FDE Lon.(m) | Jerk (m/s ³) |
|-------------------|-------------|-------------|-------------|--------------------------|
| Ind. Vel. Reg. | 6.37 | 0.67 | 13 | 0.2476 |
| L2 Cross Entropy | 1.32 | 1.95 | 2.1 | 0.2219 |
| Cost Consistency | 1.26 | 2.28 | 1.72 | 0.2148 |
| Cost Regression | 1.03 | 1.69 | 1.61 | 0.2106 |
| Demo Cost | 0.98 | 1.29 | 1.67 | 0.2030 |

V. CONCLUSION

In this work, we found an efficient multi-modal prediction result utilization method for local planning by unifying it together with other driving contexts and diagnosing it as RiskMap. An interpretable and hands-free parameter tuning planner is adopted to demonstrate the utilization and efficiency of RiskMap. We proposed the training and planning framework and analyzed the efficiency of model modules

| Method (5s) | Planning Error(m) | | Prediction Error(m) | |
|--------------------|-------------------|---------------|---------------------|---------------|
| | ADE | FDE | ADE | FDE |
| MM-Decoder | 1.6737 | 4.9665 | 1.3968 | 3.3180 |
| DIPP | 1.6945 | 4.2801 | 1.4791 | 3.4029 |
| Vector Field(ours) | 1.6642 | 4.3923 | 1.3830 | 3.1595 |

and training tools. This model can be further used in driver behavior analysis and customized agent behavior in simulators. However, the effectiveness of the use of optimization-based methods needs to be validated in future works. The learning-based planners are also supposed to have better generalizability as RiskMap offers extracted expressions of map information.

REFERENCES

- [1] Z. Lu, H. Pu, F. Wang, Z. Hu, and L. Wang, "The expressive power of neural networks: A view from the width," in *Advances in Neural Information Processing Systems*, I. Guyon, U. V. Luxburg, S. Bengio, H. Wallach, R. Fergus, S. Vishwanathan, and R. Garnett, Eds., vol. 30. Curran Associates, Inc., 2017. [Online]. Available: <https://proceedings.neurips.cc/paper/2017/file/32cbf687880eb1674a07bf717761dd3a-Paper.pdf>
- [2] S. Casas, A. Sadat, and R. Urtasun, "Mp3: A unified model to map, perceive, predict and plan," in *Proc. of the IEEE/CVF Conference on Computer Vision and Pattern Recognition*, 2021, pp. 14 403–14 412.
- [3] R. Mahjourian, J. Kim, Y. Chai, M. Tan, B. Sapp, and D. Anguelov, "Occupancy flow fields for motion forecasting in autonomous driving," *IEEE Robotics and Automation Letters*, vol. 7, no. 2, pp. 5639–5646, 2022.
- [4] S. Levine and V. Koltun, "Continuous inverse optimal control with locally optimal examples," *arXiv preprint arXiv:1206.4617*, 2012.
- [5] Z. Huang, H. Liu, J. Wu, and C. Lv, "Differentiable integrated motion prediction and planning with learnable cost function for autonomous driving," *arXiv preprint arXiv:2207.10422*, 2022.
- [6] H. Nishimura, B. Ivanovic, A. Gaidon, M. Pavone, and M. Schwager, "Risk-sensitive sequential action control with multi-modal human trajectory forecasting for safe crowd-robot interaction," in *2020 IEEE/RSJ International Conference on Intelligent Robots and Systems (IROS)*. IEEE, 2020, pp. 11 205–11 212.
- [7] Y. Lee, P. Cai, and D. Hsu, "Magic: Learning macro-actions for online pomdp planning using generator-critic," in *Robotics: Science and Systems*, 2021.
- [8] X. Weng, B. Ivanovic, and M. Pavone, "Mtp: Multi-hypothesis tracking and prediction for reduced error propagation," in *2022 IEEE Intelligent Vehicles Symposium (IV)*. IEEE, 2022, pp. 1218–1225.
- [9] T. Phan-Minh, E. C. Grigore, F. A. Boulton, O. Beijbom, and E. M. Wolff, "Covernet: Multimodal behavior prediction using trajectory sets," *CoRR*, vol. abs/1911.10298, 2019. [Online]. Available: <http://arxiv.org/abs/1911.10298>
- [10] J. Gao, C. Sun, H. Zhao, Y. Shen, D. Anguelov, C. Li, and C. Schmid, "Vectormet: Encoding HD maps and agent dynamics from vectorized representation," in *Proc. of the IEEE/CVF Conference on Computer Vision and Pattern Recognition*, 2020, pp. 11 525–11 533.
- [11] N. Deo, E. Wolff, and O. Beijbom, "Multimodal trajectory prediction conditioned on lane-graph traversals," in *5th Annual Conference on Robot Learning*, 2021.
- [12] R. Jiao, X. Liu, T. Sato, Q. A. Chen, and Q. Zhu, "Semi-supervised semantics-guided adversarial training for trajectory prediction," 05 2022.
- [13] T. Salzmann, B. Ivanovic, P. Chakravarty, and M. Pavone, "Trajectron++: Multi-agent generative trajectory forecasting with heterogeneous data for control," *CoRR*, vol. abs/2001.03093, 2020. [Online]. Available: <http://arxiv.org/abs/2001.03093>
- [14] D. Kingma and M. Welling, "Auto-encoding variational bayes," 12 2014.
- [15] D. Zhu, M. A. Zahran, L. E. Li, and M. Elhoseiny, "Motion forecasting with unlikelihood training in continuous space," 2021.
- [16] J. Cheng, R. Xin, S. Wang, and M. Liu, "Mpn: Multi-policy neural planner for urban driving," in *IEEE/RSJ Int. Conf. Intell. Rob. Sys. (IROS)*. IEEE, 2022.
- [17] J. Jiao, H. Wei, T. Hu, X. Hu, Y. Zhu, Z. He, J. Wu, J. Yu, X. Xie, H. Huang, R. Geng, L. Wang, and M. Liu, "Fusionportable: A multi-sensor campus-scene dataset for evaluation of localization and mapping accuracy on diverse platforms," 2022.
- [18] H. Moravec and A. Elfes, "High resolution maps from wide angle sonar," in *Proceedings. 1985 IEEE International Conference on Robotics and Automation*, vol. 2, 1985, pp. 116–121.
- [19] T. Gilles, S. Sabatini, D. Tsishkou, B. Stanciulescu, and F. Moutarde, "HOME: heatmap output for future motion estimation," *CoRR*, vol. abs/2105.10968, 2021. [Online]. Available: <https://arxiv.org/abs/2105.10968>
- [20] R. Liu, J. Wang, and B. Zhang, "High definition map for automated driving: Overview and analysis," *The Journal of Navigation*, vol. 73, no. 2, pp. 324–341, 2020.
- [21] S. Lefèvre, D. Vasquez, and C. Laugier, "A survey on motion prediction and risk assessment for intelligent vehicles," *ROBOMECH journal*, vol. 1, no. 1, pp. 1–14, 2014.
- [22] Z. Huang, W. Schwarting, A. Pierson, H. Guo, M. Ang, and D. Rus, "Safe path planning with multi-model risk level sets," in *2020 IEEE/RSJ International Conference on Intelligent Robots and Systems (IROS)*. IEEE, 2020, pp. 6268–6275.
- [23] A. Pierson, W. Schwarting, S. Karaman, and D. Rus, "Navigating congested environments with risk level sets," in *2018 IEEE International Conference on Robotics and Automation (ICRA)*. IEEE, 2018, pp. 5712–5719.
- [24] Y. Pan, Q. Lin, H. Shah, and J. M. Dolan, "Safe planning for self-driving via adaptive constrained ilqr," in *2020 IEEE/RSJ International Conference on Intelligent Robots and Systems (IROS)*, 2020, pp. 2377–2383.
- [25] N. Ab Azar, A. Shahmansoorian, and M. Davoudi, "From inverse optimal control to inverse reinforcement learning: A historical review," *Annual Reviews in Control*, vol. 50, pp. 119–138, 2020.
- [26] F. Yaman, V. G. Yakhno, and R. Potthast, "A survey on inverse problems for applied sciences," *Mathematical problems in engineering*, vol. 2013, 2013.
- [27] F. Ornelas, E. N. Sanchez, and A. G. Loukianov, "Discrete-time inverse optimal control for nonlinear systems trajectory tracking," in *49th IEEE Conference on Decision and Control (CDC)*. IEEE, 2010, pp. 4813–4818.
- [28] S. Levine and V. Koltun, "Continuous inverse optimal control with locally optimal examples," *arXiv preprint arXiv:1206.4617*, 2012.
- [29] S. Levine, Z. Popovic, and V. Koltun, "Nonlinear inverse reinforcement learning with gaussian processes," *Advances in neural information processing systems*, vol. 24, 2011.
- [30] W. Zeng, W. Luo, S. Suo, A. Sadat, B. Yang, S. Casas, and R. Urtasun, "End-to-end interpretable neural motion planner," in *Proc. of the IEEE/CVF Conference on Computer Vision and Pattern Recognition*, 2019, pp. 8660–8669.
- [31] A. Cui, S. Casas, A. Sadat, R. Liao, and R. Urtasun, "Lookout: Diverse multi-future prediction and planning for self-driving," in *Proc. of the IEEE/CVF International Conference on Computer Vision*, 2021, pp. 16 107–16 116.
- [32] M. Werling, J. Ziegler, S. Kammel, and S. Thrun, "Optimal trajectory generation for dynamic street scenarios in a frenet frame," in *2010 IEEE International Conference on Robotics and Automation*, 2010, pp. 987–993.
- [33] M. McNaughton, C. Urmson, J. M. Dolan, and J.-W. Lee, "Motion planning for autonomous driving with a conformal spatiotemporal lattice," in *2011 IEEE International Conference on Robotics and Automation*. IEEE, 2011, pp. 4889–4895.
- [34] J. Houston, G. Zuidhof, L. Bergamini, Y. Ye, L. Chen, A. Jain, S. Omari, V. Iglovikov, and P. Ondruska, "One thousand and one hours: Self-driving motion prediction dataset," in *Conference on Robot Learning*. PMLR, 2021, pp. 409–418.
- [35] I. Loshchilov and F. Hutter, "Decoupled weight decay regularization," in *International Conference on Learning Representations*, 2018.
- [36] M. Bansal, A. Krizhevsky, and A. Ogale, "ChauffeurNet: Learning to drive by imitating the best and synthesizing the worst," in *Rob. Sci. Systems*, Freiburg/Breisgau, Germany, June 2019.